

## Supporting Information

### Mechanistic and thermodynamical aspects of pyrene based fluorescent probe to detect picric acid

Bidyut Kumar Kundu,<sup>a</sup> Pragti,<sup>a</sup> Reena,<sup>a</sup> Shaikh M. Mobin<sup>a</sup> and Suman Mukhopadhyay<sup>\*a,b</sup>

<sup>a</sup>Discipline of Chemistry, School of Basic Sciences, Indian Institute of Technology Indore,  
Khandwa Road, Simrol, Indore 453552, India. Tel: +91 731 2438 735 Fax: +91 731 2361 482

<sup>b</sup>Discipline of Biosciences and Biomedical Engineering, School of Engineering, Indian Institute of  
Technology Indore, Khandwa Road, Simrol, Indore 453552, India.

\*Contact E-mail: [suman@iiti.ac.in](mailto:suman@iiti.ac.in); Fax: +91 731 2361; Tel: +91 731 2438 735

#### Table of Contents

List of Acronyms .....	ESI 2
Experimental Section .....	ESI 3-6
List of Figures .....	ESI 7-18
List of Tables .....	ESI 19-23
References .....	ESI 24

## List of Acronyms

<i>Entry</i>	<i>Significance</i>	<i>Entry</i>	<i>Significance</i>
<b>PTC</b>	(2E/Z)-2-(9-Pyrenylmethylene)hydrazide-2-ThiopheneCarboxylic acid	<b>PL/ FL</b>	Photo luminance/ Fluorescence
<b>ESIPT</b>	Excited state intra/ intermolecular proton transfer	<b>Aq.</b>	Aqueous
<b>DFT/ TDDFT</b>	Density functional Theory/ Time dependent density functional Theory	<b>FRET</b>	Fluorescence resonance energy transfer
<b>NMR</b>	Nuclear magnetic resonance	<b>XRD</b>	X-ray diffraction
<b>ESI-MS</b>	Electrospray ionization mass spectrometry	<b>UV-Vis</b>	Ultraviolet-Visible
<b>FTIR</b>	Fourier transformed infra-red	<b>Conc.</b>	Concentration
<b>nM</b>	Nano molar	<b>h/ hrs.</b>	Hour/ Hours
<b>LOD</b>	Limit of detection/ detection limit	<b>r.t.</b>	Room temperature
<b>CHEF</b>	Chelation-enhanced fluorescence	<b>equiv.</b>	Equivalents
<b>MLCT</b>	Metal to ligand charge transfer	<b>eqn.</b>	Equation
<b>PET</b>	Photo induced electron/energy transfer	<b>ns/ min</b>	Nano seconds/ minutes
<b>HPLC</b>	High performance liquid chromatography	<b>[M<sup>n+</sup>]</b>	Concentration of metal
<b>TCSPC</b>	Time-correlated single photon counting	<b>AIE</b>	Aggregation Induced Emission
<b>LUMO</b>	Lowest unoccupied molecular orbital	<b>HOMO</b>	Highest occupied molecular orbital
<b><math>\lambda_{ex}</math> or <math>\lambda_{em}</math></b>	Excitation or emission wavelength maximum	<b>ICT</b>	Intramolecular charge transfer
<b>NACs</b>	Nitro aromatic compounds	<b>ACN</b>	Acetonitrile

## Experimental Section

### Section S1. Materials

All reagents and solvents were purchased from commercial sources and used as received unless stated otherwise. Mili-Q water was used throughout the experiment. The solutions of the metal ions were prepared from their nitrate and chloride salts.

### Section S2. Apparatus and Procedures

Absorption spectra were performed on a Varian UV-Vis spectrophotometer (Model: Cary 100). Fluorescence emission spectra were recorded at  $25.0 \pm 0.2$  °C on a Fluoromax-4p spectrofluorometer from Horiba JobinYvon (Model: FM-100) using a quartz cuvette with a path length of 2 cm.  $^1\text{H}$  and  $^{13}\text{C}$  NMR spectra were recorded on an AVANCE III 400 Ascend Bruker BioSpin machine at ambient temperature with tetramethylsilane (TMS, 0.00 ppm) as an internal standard. Elemental analysis was recorded on a ThermoFlash 2000 elemental analyzer. ESI-Mass spectra were recorded on a Bruker micrOTOF-Q II by positive-mode electrospray ionization. Infrared spectra ( $4000$  to  $500\text{ cm}^{-1}$ ) were recorded with a BRUKER TENSOR 27 instrument in KBr pellets. A HORIBA Jobin Yvon picosecond time-correlated single photon counting (TCSPC) spectrometer (model Fluorocube-01-NL) was used for recording PL decays. The samples were excited at 405 nm by a picoseconds diode laser (model Pico Brite-405L) at a magic angle of  $54.7^\circ$  by a photomultiplier tube (TBX-07C) to collect the PL decays. The instrument response function (IRF, FWHM  $\sim 140$  ps) was recorded using a dilute scattering solution, and IBH DAS 6.0 software was used to analyze the PL decays by the iterative reconvolution method. The goodness of the fit was judged by reduced  $\chi$ -square ( $\chi^2$ ) value. Hand held camera was used to take the photos of UV-chamber as well as in day light.

### Section S3. Preparation of Solutions for photophysical measurements

- **UV-visible and fluorescence titration**

To record UV-vis spectra, 1.0 mM solution (stock solution) was prepared by dissolving 0.01 mmol of chemosensor PTC (3.54 mg) in 10 mL of acetonitrile, followed by dilution to get 0.04 mM of working solution. 40  $\mu\text{L}$  of working solution was taken and diluted up to 2 mL to get 0.08  $\mu\text{M}$  solution.

Additionally, 0.1 mmol of  $\text{Cu}(\text{NO}_3)_2 \cdot 3\text{H}_2\text{O}$  (24.1 mg) was dissolved in deionized  $\text{H}_2\text{O}$  (10 mL) to obtain a 10 mM solution. All the metal ions are added such a way that the conc. of overall solution during experiments become 0.8  $\mu\text{M}$ . After mixing both the solution of chemosensor and metal ion, it was shaken for one minute and UV-visible spectra of the resultant solution were recorded.

Similar procedure was followed for the preparation of explosive material's solution using water and sometimes-other polar solvents according to the experimental requirement. Furthermore, the concentration of PTC sometimes selectively chosen according the experimental requirement during PL spectroscopy.

- **Determination of association constant**

Benesi-Hildebrand (B-H) plot was used to evaluate the binding constants of the corresponding metal complexes using the following eqn. s(i):<sup>1</sup>

$$1/(F - F_0) = 1/\{K(F_{\max} - F_0)C\} + 1/(F_{\max} - F_0) \quad \dots \quad \text{s(i)}$$

Where,  $F_0$  is the FL intensity of probe PTC at the emission maximum ( $\lambda_{\text{ex}} = 368 \text{ nm}$ ,  $\lambda_{\text{em}} = 425 \text{ nm}$ ).  $F$  is the value of various concentration dependent wavelength emission maximum, the maximum emission intensity is denoted by  $F_{\max}$ , the ratio of intercept to slope after fitting into the linear plot gives the value of  $K$  i.e. the binding constant ( $M^{-1}$ ), and  $C$  denotes the conc. of the  $\text{Cu}^{2+}$  utilized throughout the series of titration. The Benesi-Hildebrand plot of  $(F_{\max} - F_0)/(F - F_0)$  vs.  $1/[Cu^{2+}]$  gives the value of binding constant.

- **Limit of Detection (LOD) for PA**

Eqn. S(ii) was used to calculate the LOD value based on the fluorescence emission for PA.<sup>2</sup>

$$\text{Detection limit (DL)} = 3\sigma/k \quad \dots \quad \text{s(ii)}$$

Where,  $\sigma$  stands for the standard deviation ( $S_d$ ) of the blank measurement, and  $k$  denotes the slope. Slope is obtained from the linear fit plot of FL intensity changes versus concentration of PA or  $\text{Cu}^{2+}$  added to the probe at a particular wavelength.

- **Calculation of Excited-State Lifetimes**

Equations s(iii) and s(iv) were fitted to get an idea about the time-resolved emission decays where the decays of the compounds were evaluated using a tri-exponential function:<sup>3</sup>

$$F(t) = \sum_{i=1}^2 a_i \exp\left(-\frac{t}{\tau_i}\right) \quad \dots \quad \text{s(iii)}$$

Where,  $F(t)$  is the FL decay at normalized condition,  $\alpha_i$  is the pre-exponential factor, and  $a_1$  and  $a_2$  denotes the normalized amplitude having decay component  $\tau_1$  and  $\tau_2$  respectively. Eqn. (iv) gives the value of average lifetime (in ns):

$$\langle \tau \rangle = \sum_{i=1}^2 a_i \tau_i \quad \dots \quad \text{s(iv)}$$

Where,  $a_i$  is the contribution of the  $i^{\text{th}}$  decay component, and  $a_i = \alpha_i / \sum \alpha_i$ .

- **Fluorescence Quantum Yield**

Coumarin 152 dye ( $\Phi_R = 0.09$  in methanol) was used as reference to estimate the quantum yield (QY) values of different analytes<sup>4</sup> by using the eqn. s(v):<sup>5</sup>

$$\Phi_s = \frac{Abs_R}{Abs_S} \times \frac{Area_S}{Area_R} \times \frac{\eta_S}{\eta_R} \times \Phi_R \quad \dots \quad \dots S(\nu)$$

Where 'Φ' denotes the fluorescence QY, 'Area' terms denote the integration of the fluorescence curve, 'Abs' denotes optical density and the refractive index as 'η' (η = 1.3284 for MeOH solvent medium). Subscripts 'R' and 'S' stand for the respective parameters belonging to the experimental reference as well as the sample.

- **Density Functional Theory (DFT)**

For better understanding about the favorable pathways for the formation of metal complexes, MO based geometries and energies were calculated by using the Gaussain-09 programs.<sup>6</sup> Restriction free Gas phase geometries for compounds and the sensing mechanism were fully optimized under symmetrical conditions. The singlet ground states (S<sub>0</sub>) of PTC and complexes were optimized using DFT methods by mixing the Hartree-Fock-type theory with Becke's three parameterized Lee-Yang-Parr (B3LYP)<sup>7</sup> exchange functional with the 6-31G basis set.<sup>8,9</sup> Furthermore, TDDFT method has been utilized by incorporating CAMB3LYP/ 6-31+G to correlate the theoretical and experimental observation for the electronic spectra.<sup>10</sup>

#### **Section S4. Synthesis of PTC [(2E/Z)-2-(9-Pyrenylmethylene)hydrazide-2-ThiopheneCarboxylic acid)]**

The solution of thiophene-2-carboxylic hydrazide (2 mmol = 284 mg) in MeOH (10 mL) was added to a methanolic solution (30 mL) of pyrene-1-carboxaldehyde (2 mmol = 460 mg). The mixture was then refluxed for 8 h at 70 °C followed by the filtration and washed through MeOH and diethylether. The solid crystalline residue was dried over vacuum and collected for further characterization. X-ray diffraction suitable deep yellow colored single crystals were obtained after 9 days by slow evaporation in DMF solvent at room temperature.

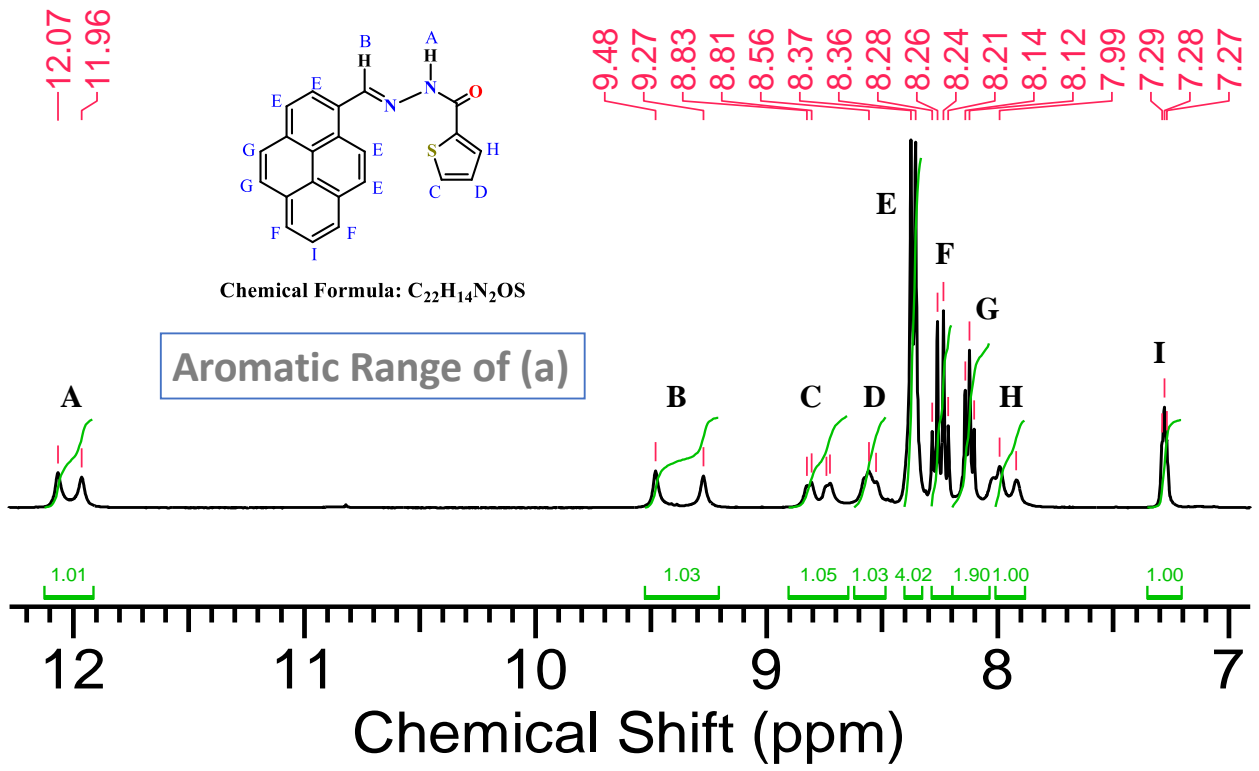
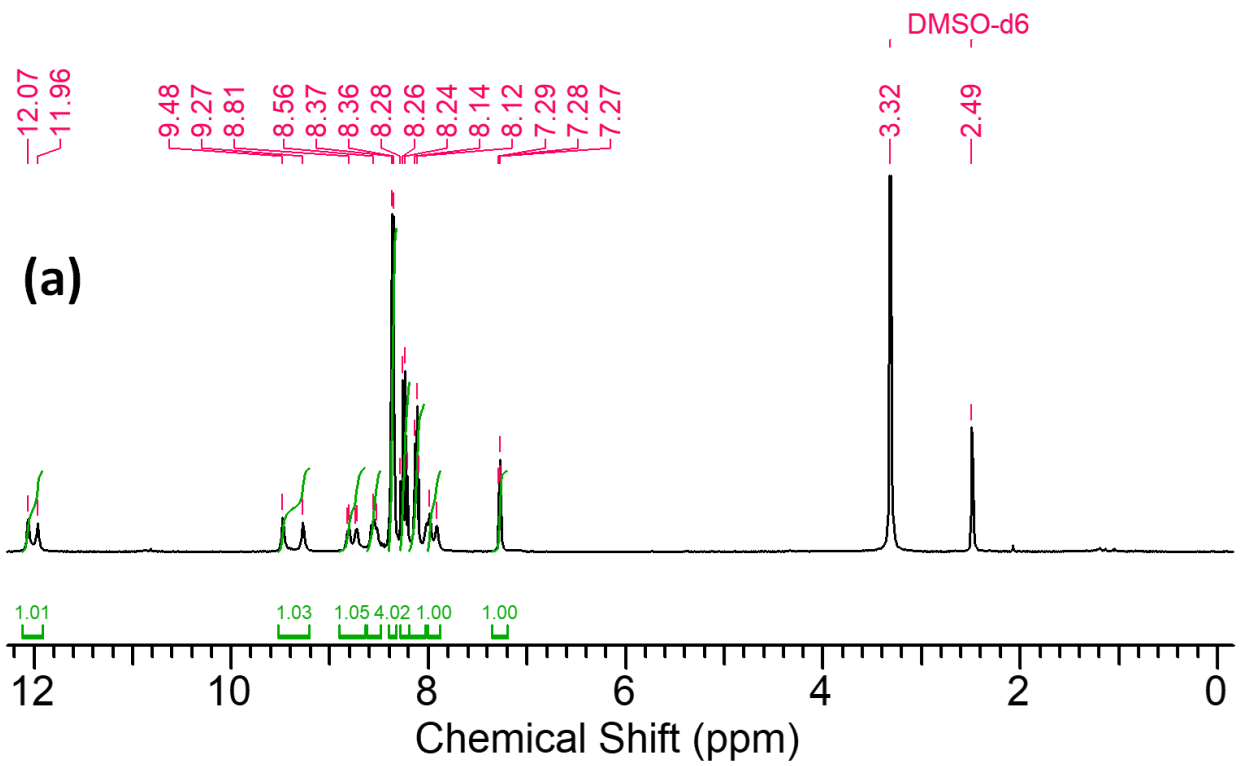
Yield: 92% (orange solid), M.p. 265-268 °C. <sup>1</sup>H NMR (400.13 MHz, 298K, D<sub>6</sub>-DMSO, δ ppm, E:Z = 1.4:1) : δ (E-isomer) = 7.29 (1H, t, Py-H), 7.99 (1H, d, Th-CH), 8.14 (2H, d, Py-H), 8.28 (2H, d, Py-H), 8.37 (4H, d, Py-H), 8.56 (1H, t, Th-CH), 8.83 (1H, d, Th-CH), 9.48 (1H, s, Py-CH=N), 12.07 (1H, s, exchangeable C=O-NH) ppm; (Z-isomer) = 7.27 (1H, t, Th- Py-H), 7.92 (1H, d, Th-CH), 8.10 (2H, d, Py-H), 8.21 (2H, d, Py-H), 8.36 (4H, d, Py-H), 8.55 (1H, t, Th-CH), 8.73 (1H, d, Th-CH), 9.27 (1H, s, Py-CH=N), 11.96 (1H, s, exchangeable C=O-NH) ppm (Fig. S1a); <sup>13</sup>C NMR (100.61 MHz, 298 K, D<sub>6</sub>-DMSO, δ ppm): (E/Z-isomer) = δ 124, 126, 127, 128, 129, 130, 131, 132, 135, 142, 146, 158, 161 (Fig. S1b). FT-IR (KBr, cm<sup>-1</sup>): 3220 and 3063 (N-H), 1635 (C=O), 1560 (C=N) (Fig. S2). Anal. Calcd (%) for C<sub>22</sub>H<sub>14</sub>N<sub>2</sub>OS: C, 74.55; H, 3.98; N, 7.90; O, 4.51; S, 9.05. Found: C, 74.29; H, 3.57; N, 7.94; S, 8.93 %. HRMS in HPLC MeOH (+, m/z): (C<sub>22</sub>H<sub>14</sub>N<sub>2</sub>OS + Na)<sup>+</sup>: 377.0719 (100%) (Fig. S3).

## Section S5. Description of Single Crystal XRD Analysis

Yellowish block like single crystals suitable for X-ray analysis of chemosensor, PTC were obtained from DMF within four days. The structure elucidation reveals monoclinic space group of the compound (P 21/c). The crystallized compound with approximate dimension of 0.330 x 0.260 x 0.210 mm, was used to measure the X-ray intensity data. The Bruker SAINT Software package<sup>11</sup> were used to integrate the data of a monoclinic unit cell generating a total no. of 15958 reflections using a maximum  $\theta$  angle of 25.24°, of which 4083 were independent.

The final cell constants of  $a = 13.6604(4) \text{ \AA}$ ,  $b = 10.0147(3) \text{ \AA}$ ,  $c = 12.6251(3) \text{ \AA}$ ,  $\alpha = 90^\circ$ ,  $\beta = 99.643(3)^\circ$ ,  $\gamma = 90^\circ$ , volume = 1702.77(8)  $\text{\AA}^3$ . The Multi-Scan method (SADABS) was introduced to correct the data effects for absorption. The ratio of minimum to maximum apparent transmission was 0.69668. The structure was solved and refined using the Bruker SHELXTL Software Package<sup>12</sup>, giving the molecular formula,  $C_{22}H_{14}N_2OS$ . The final anisotropic full-matrix least-squares refinement on  $F^2$  [30] with 235 variables converged at  $R1 = 8.49\%$ , for the observed data and  $wR2 = 24.67\%$  for all data. The goodness-of-fit was 1.083. On the basis of the final model, the calculated density was 1.382  $\text{Mg/m}^3$  and  $F(000)$ , 736  $e^-$ .

**Caution!** NACs are extremely explosive in nature and should be handled carefully and in small amounts. The explosives were handled as dilute solutions and with safety measures to avoid explosion. Use of fume hood is mandatory for each solution preparation!



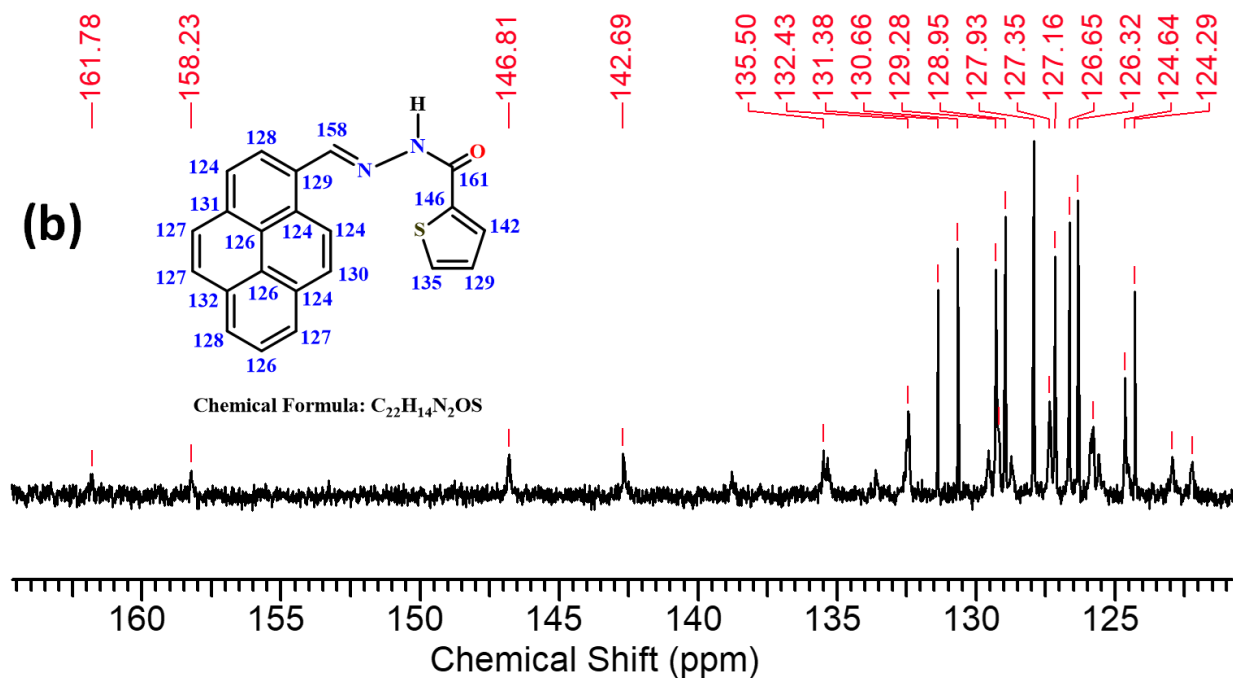


Fig. S1 (a)  $^1H$  NMR and (b)  $^{13}C$  NMR of PTC in DMSO- $d_6$  at 298K

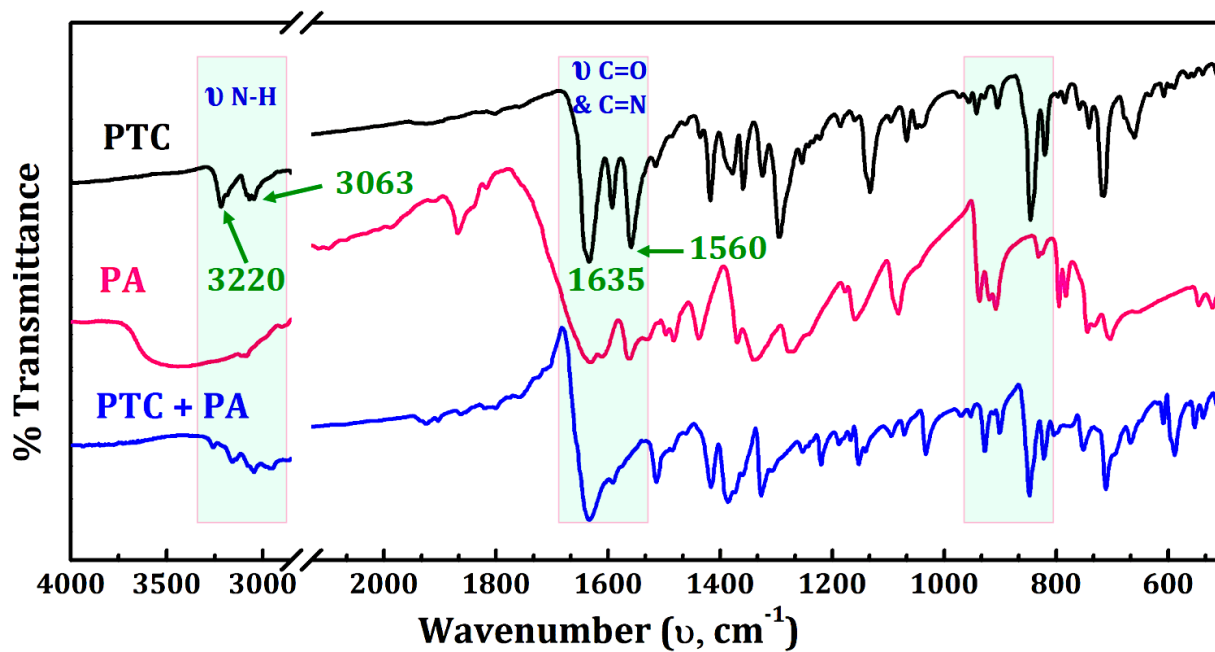
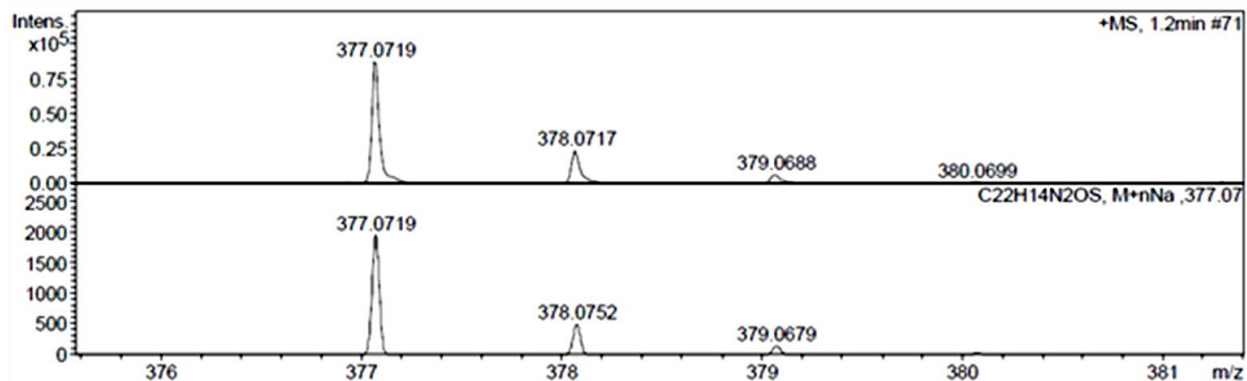
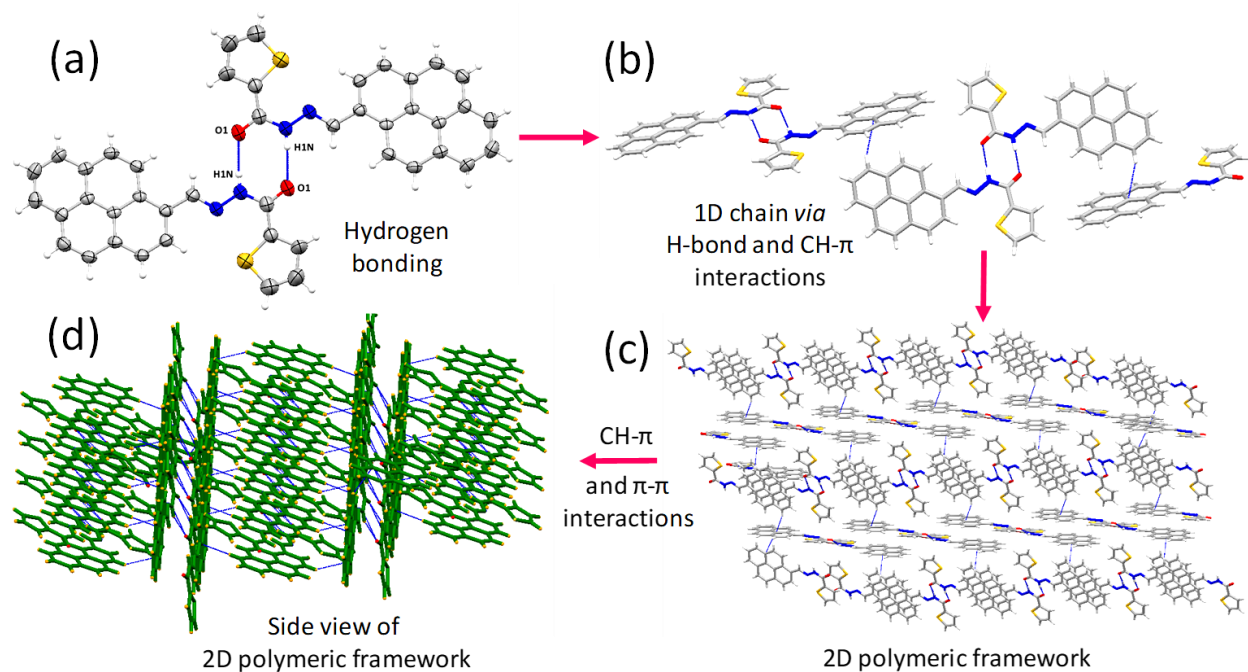


Fig. S2 FTIR stretching frequencies of PTC, PA, and the mixture of PTC and PA (in KBr pallet)<sup>13</sup>



**Fig. S3** HRMS of chemosensor, PTC in MeOH



**Fig. S4** Supramolecular interactions operating in chemosensor PTC: (a) intermolecular hydrogen bonding through two discrete molecules of PTC viz. N1-H1N...C5-O1, (b) extensive 1D polymer by H-bonding as well as CH- $\pi$  interactions, (c) 2D framework via H-bonding, CH- $\pi$ , and  $\pi$ - $\pi$  interactions, and (d) side view of (c).

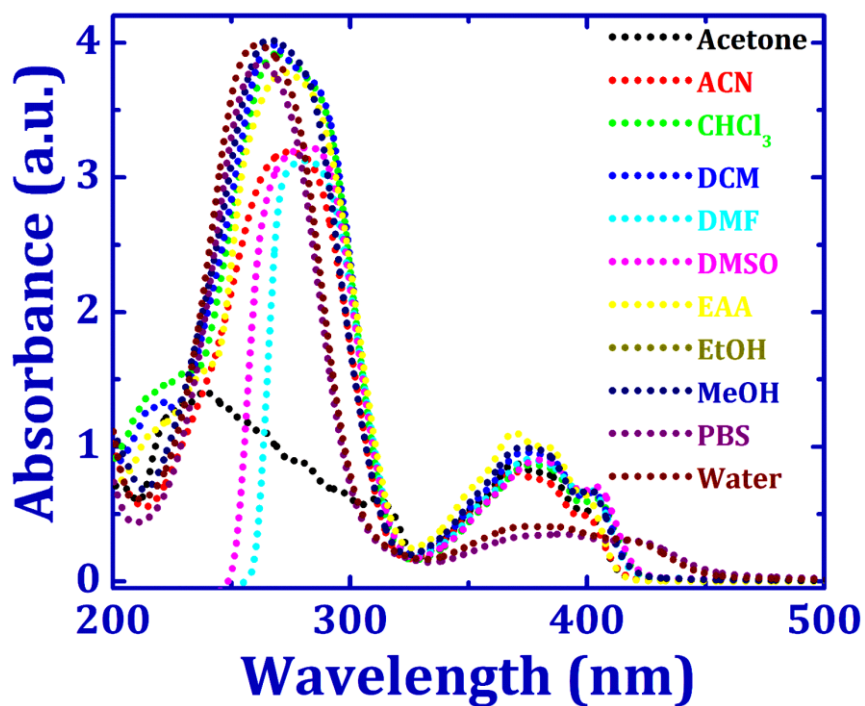


Fig. S5 Solvent dependent absorption properties of probe PTC (0.08  $\mu\text{M}$  concentration of each solution).

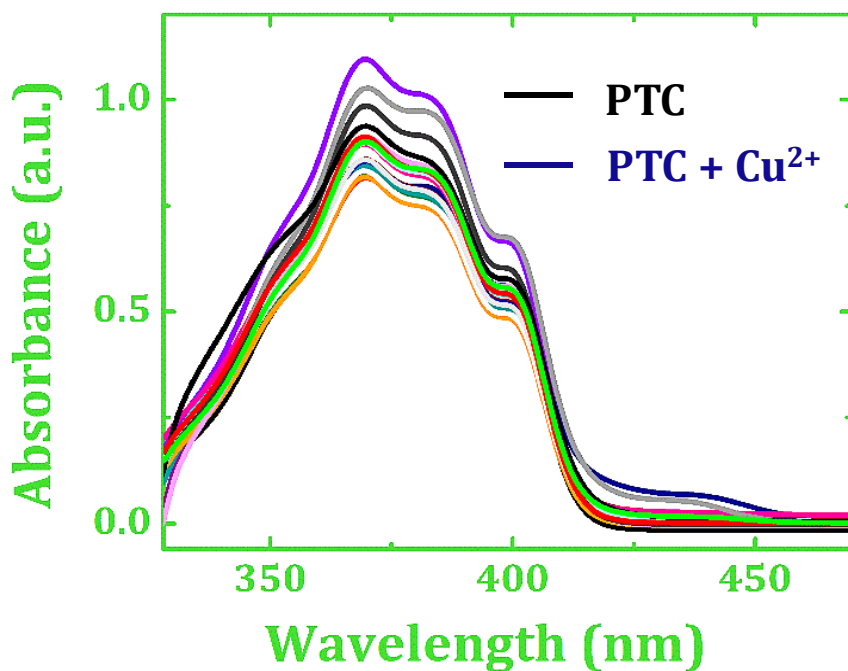


Fig. S6 The sensing behavior of PTC (0.08  $\mu\text{M}$ ) with different metal ions (0.8  $\mu\text{M}$ ), viz.,  $\text{Al}^{3+}$ ,  $\text{Cr}^{3+}$ ,  $\text{Mn}^{2+}$ ,  $\text{Fe}^{3+}$ ,  $\text{Co}^{2+}$ ,  $\text{Ni}^{2+}$ ,  $\text{Cu}^{2+}$ ,  $\text{Zn}^{2+}$ ,  $\text{Cd}^{2+}$ ,  $\text{Gd}^{3+}$ ,  $\text{Hg}^{2+}$ ,  $\text{Pb}^{2+}$ ,  $\text{Pd}^{2+}$ ,  $\text{Li}^{+}$ ,  $\text{Na}^{+}$ ,  $\text{K}^{+}$ ,  $\text{Mg}^{2+}$ , and  $\text{Ba}^{2+}$ , as its nitrate salt was investigated in acetonitrile-water by UV-visible measurements.

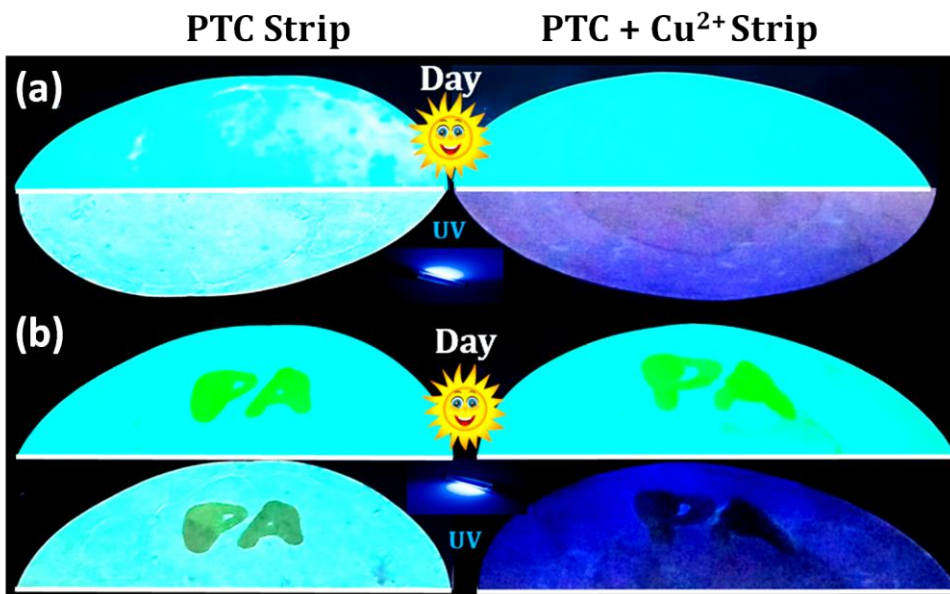


Fig. S7 Naked eye distinction of (a) PTC and PTC + Cu<sup>2+</sup> under ultraviolet light, and (b) paper strip test of picric acid in both PTC and PTC + Cu<sup>2+</sup> under visible and ultraviolet light.

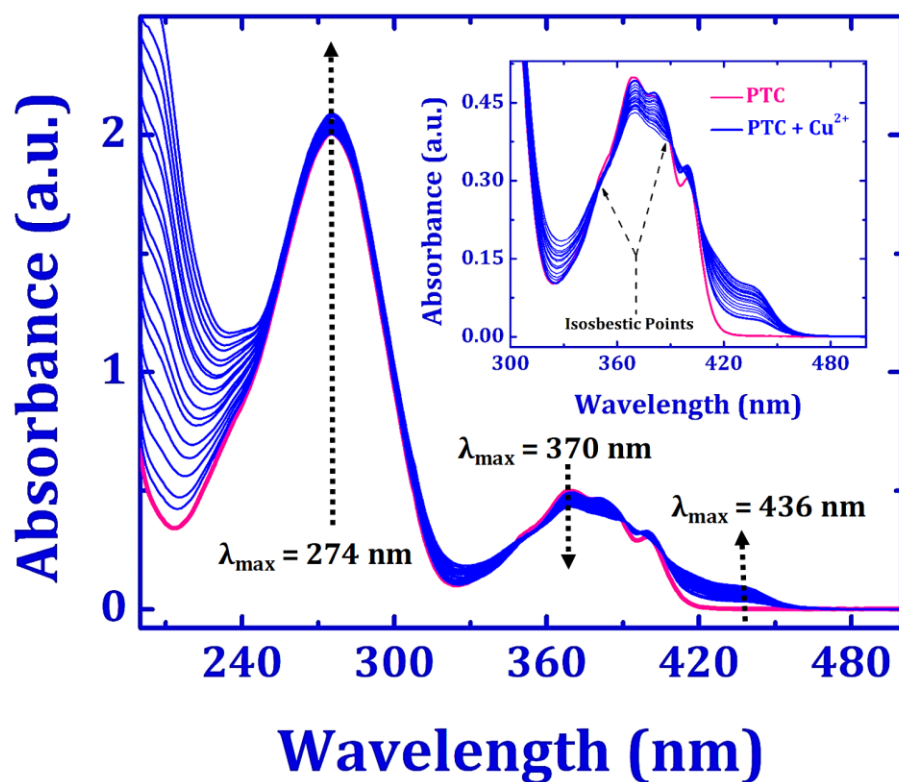


Fig. S8 UV-visible spectroscopic titration of PTC (0.04  $\mu\text{M}$ ) in the wide range of Cu<sup>2+</sup> ion concentration (0.1-0.4  $\mu\text{M}$ ) in CH<sub>3</sub>CN solvent.

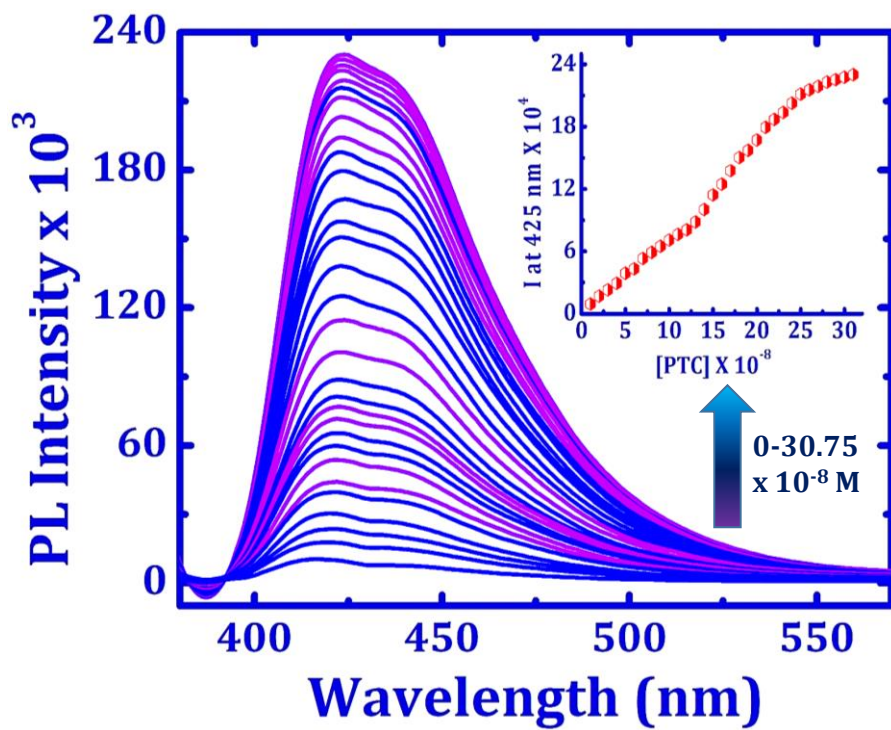
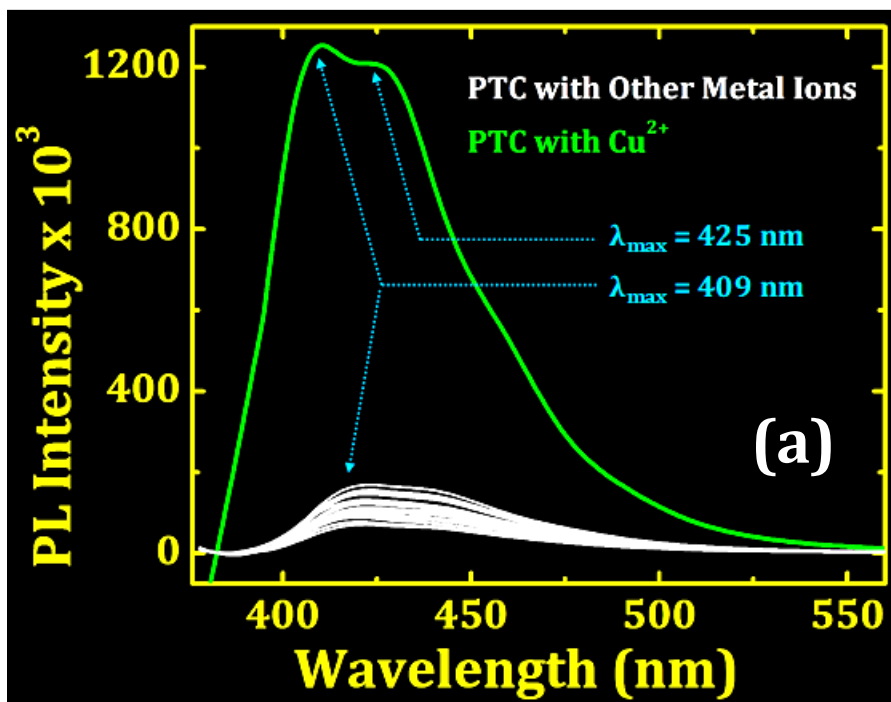
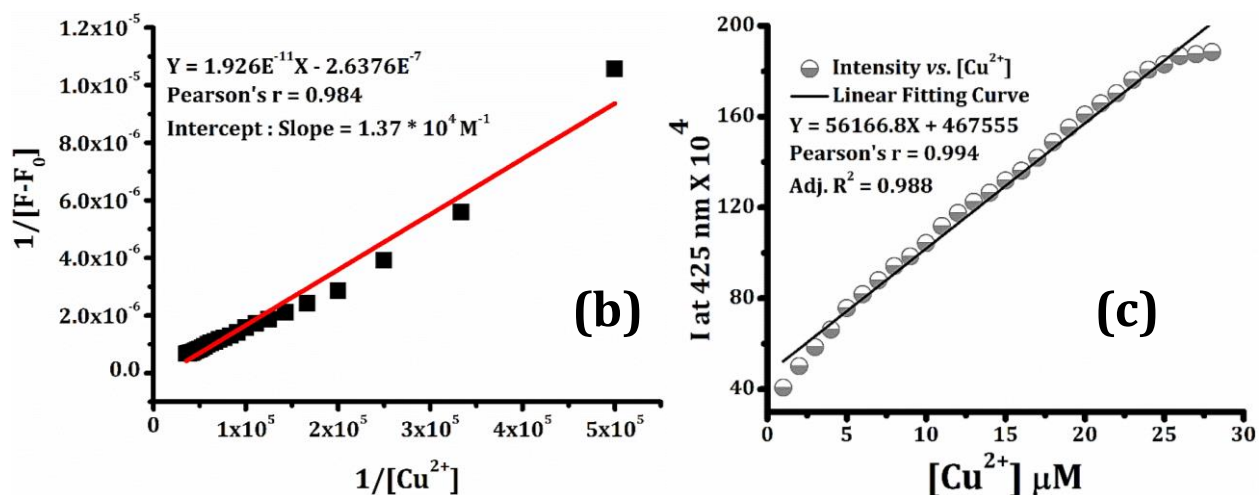
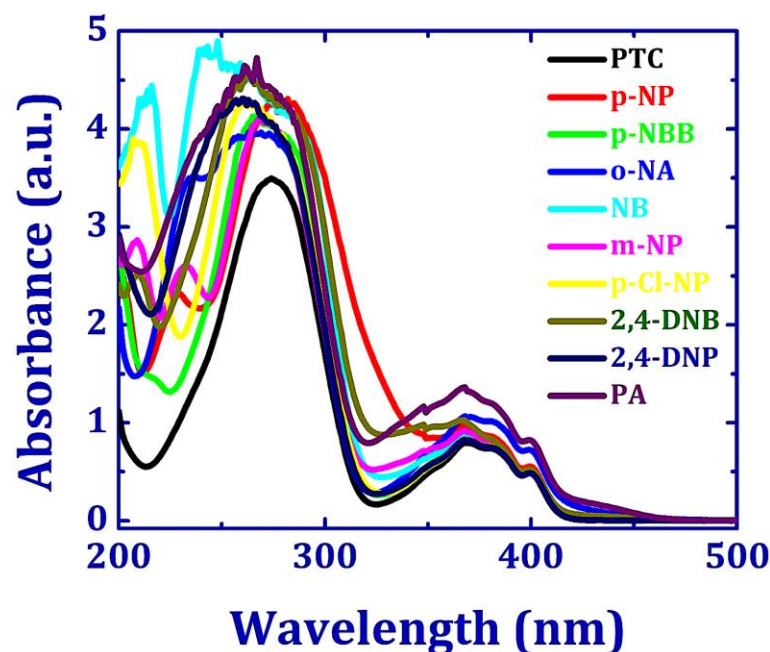


Fig. S9 Concentration dependent photoluminescence spectra of PTC (0-307.5 nM).

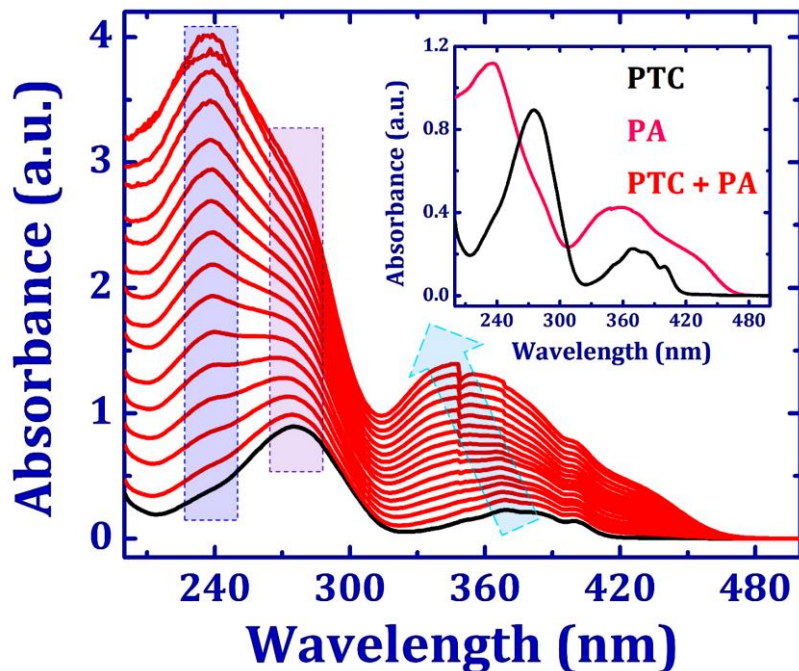




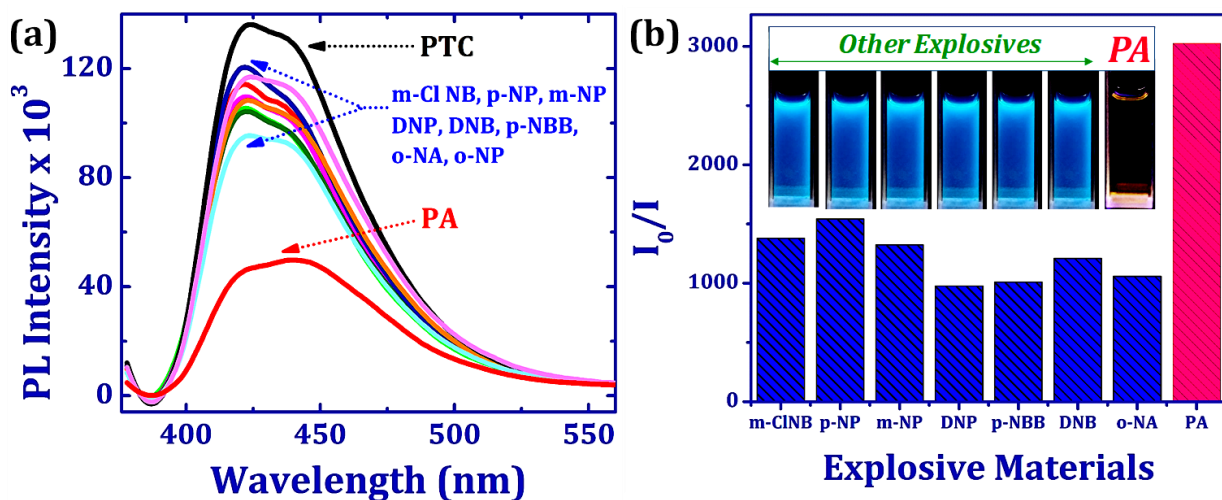
**Fig. S10** (a) Selective fluorescence profile of PTC (0.1  $\mu\text{M}$  in acetonitrile) and with other metal ions (1.0  $\mu\text{M}$ ). (b) Benesi-Hildebrand (B-H) plot for the determination of association constant ( $K_a$  in  $\text{M}^{-1}$ ) through FL spectroscopy. (c) Determination of LOD value for  $\text{Cu}^{2+}$  detection.



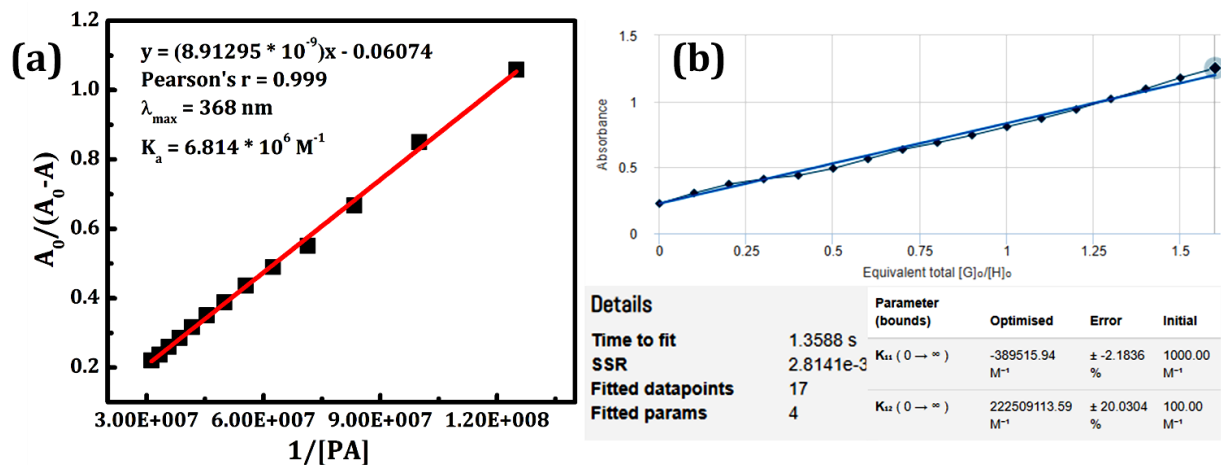
**Fig. S11** Absorption spectra of PTC after addition of various nitro explosives (0.08  $\mu\text{M}$  in acetonitrile solvent). Entry sequences from top to bottom: probe (PTC), PTC + p-nitrophenol (p-NP), PTC + p-nitrobenzylbromide (p-NNB), PTC + o-nitrophenol (o-NP), PTC + nitrobenzene (NB), PTC + m-nitrophenol (m-NP), PTC + p-chloronitrophenol (p-Cl-NP), PTC + 2,4-dinitrobenzene (2,4-DNB), PTC + 2,4-dinitrophenol (2,4-DNP), PTC + 2,4,6-trinitrophenol (PA).



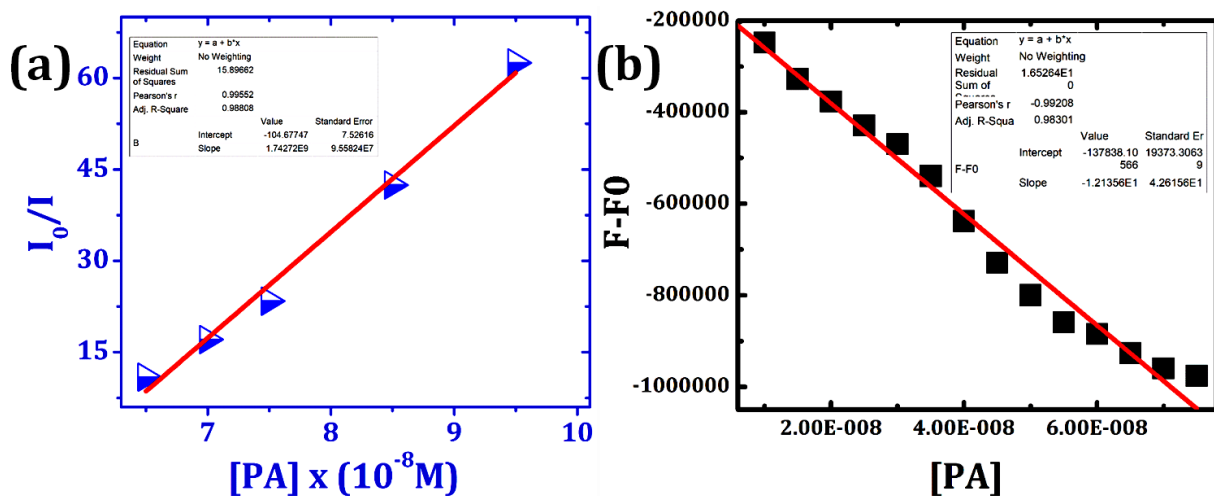
**Fig. S12** UV-visible titration of PTC (0.02  $\mu\text{M}$  in acetonitrile solvent) in presence of PA (0-0.0032  $\mu\text{M}$ ). Inset: Absorbance spectra of PTC and PA (0.02  $\mu\text{M}$  in acetonitrile solvent).



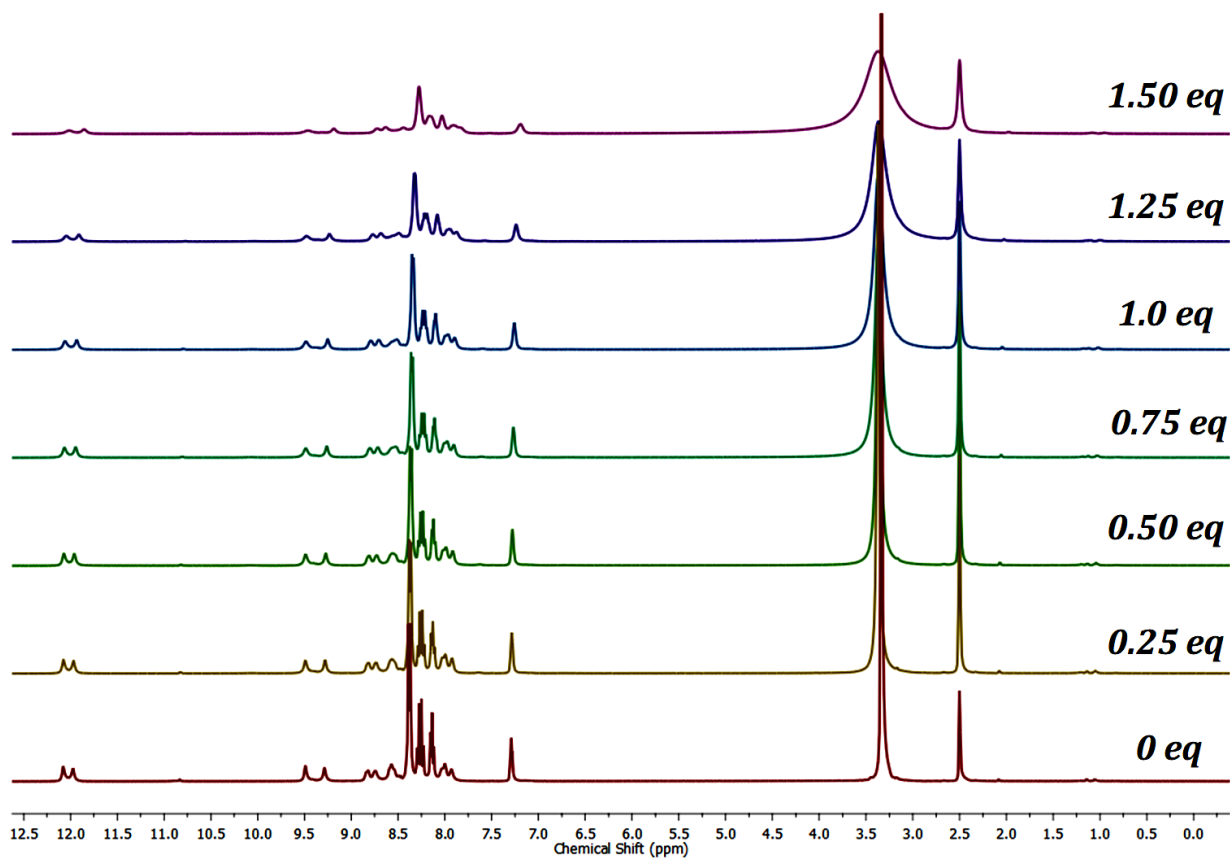
**Fig. S13** (a) Fluorescence quenching profile of 0.08  $\mu\text{M}$  of PTC in presence of various nitroaromatic explosives (NACs) having concentration of 50 nM. (b) Histogram for the interference of several NACs towards the detection of PA having emission at 425 nm.



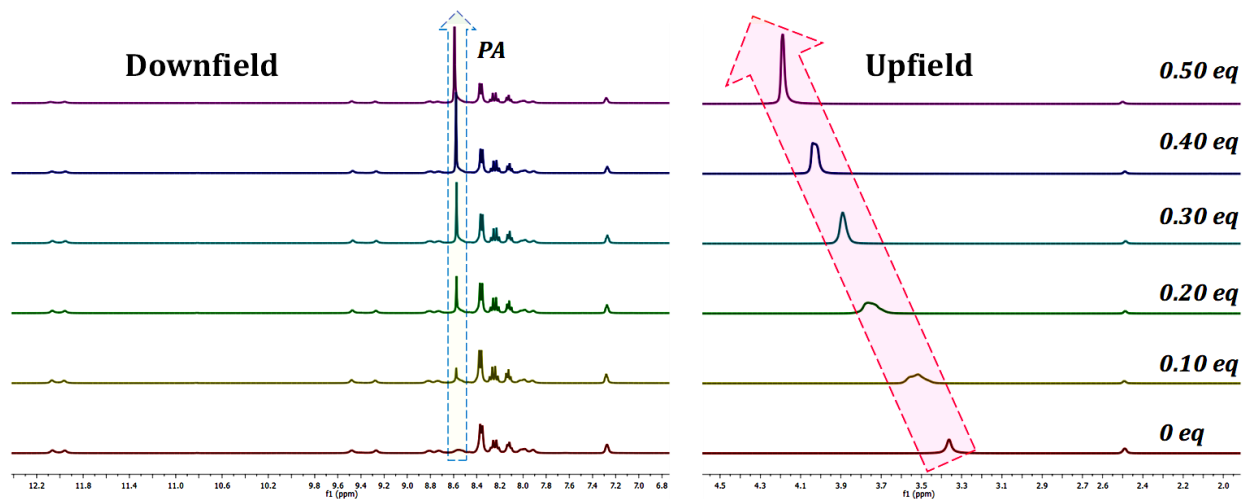
**Fig. S14** (a) Benesi-Hildebrand (B-H) plot for the determination of association constant ( $K_a$  in  $\text{M}^{-1}$ ) through UV-Vis titration method, and (b) corresponding online fitted data having error < 3% via 'BindFit v0.5- Supramolecular' server.



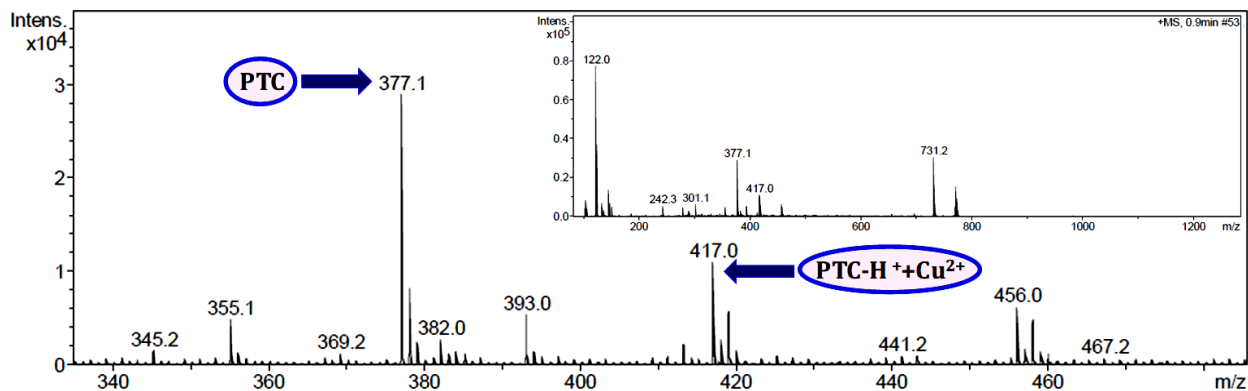
**Fig. S15** (a) Stern-Volmer plot presenting linearity at higher concentration of PA, and (b) Plot of the intensity a mixture of sensor PTC (F-F0) and [PA] in acetonitrile; where F is the fluorescence intensity of PTC upon gradual addition of PA, F0 is the initial FL intensity in absence of PA, and [PA] is the molar concentration of picric acid. LOD was calculated as per reported literature.<sup>14</sup>



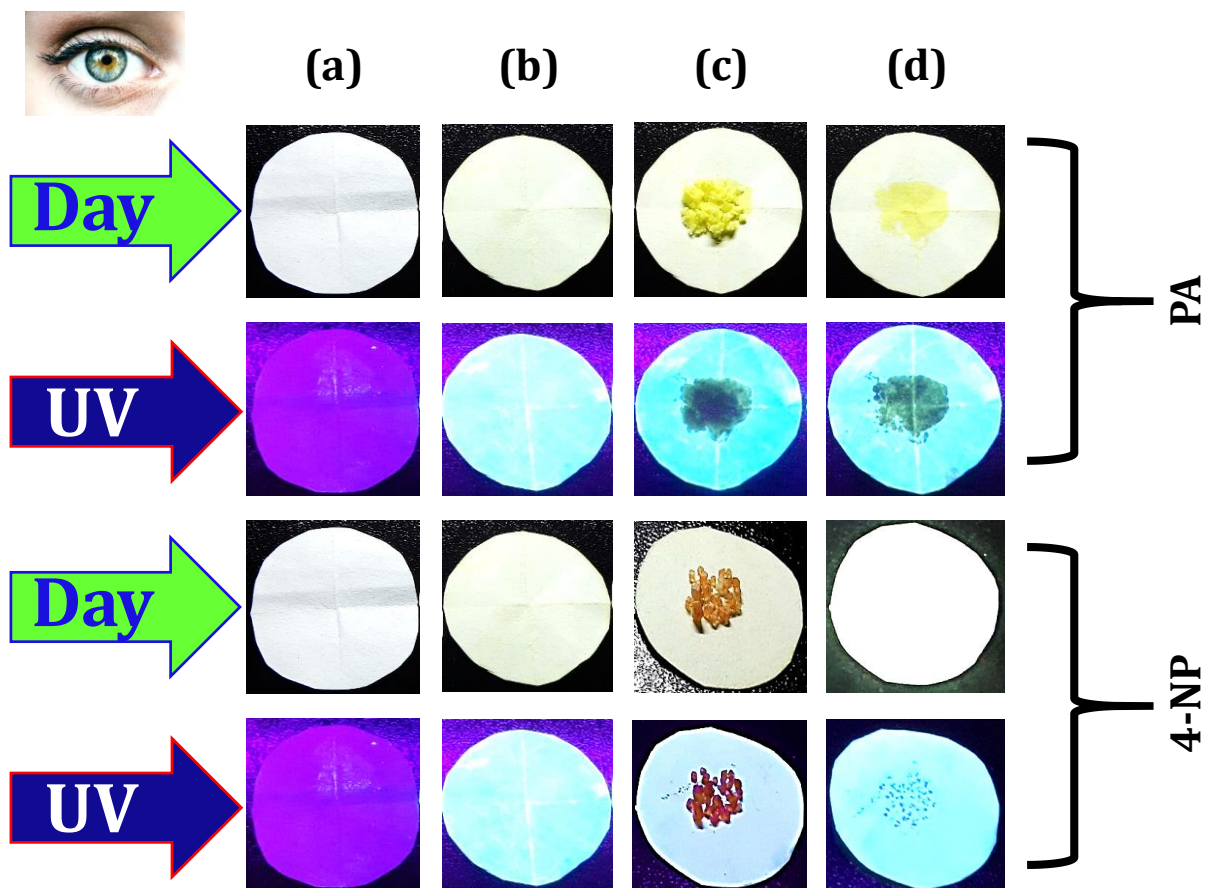
**Fig. S16**  $^1\text{H}$  NMR chart (400.13 MHz, 298K,  $\text{D}_6\text{-DMSO}$ , 0.5 mL,  $\delta$  ppm) of PTC (5 mg) by varying the concentration of  $\text{Cu}^{2+}$  ion.



**Fig. S17** Different region (shielding and deshielding) of  $^1\text{H}$  NMR spectra (400.13 MHz, 298K,  $\text{D}_6\text{-DMSO}$ , 0.5 mL,  $\delta$  ppm) of PTC (5 mg) by varying the concentration of PA.



**Fig. S18** ESI-MS spectra showing complex formation equilibrium during titration of PTC with Cu<sup>2+</sup> ion in HPLC acetonitrile medium.



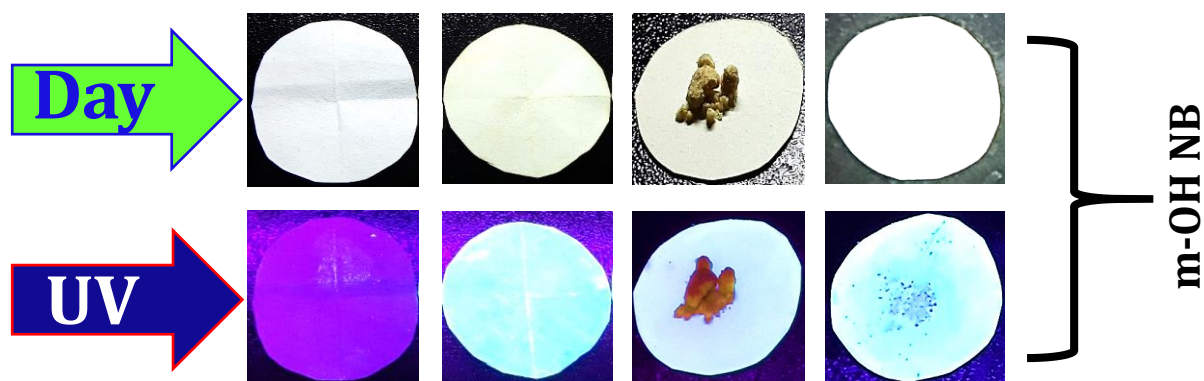


**Fig. S19** Solid state identification of some NACs through paper strip experiment. (a) Blank strip, (b) PTC strip, (c) PTC strip including solid state explosives, (d) PTC strip excluding solid state explosives. Images were taken after in contact with PTC-explosives for 60 seconds. (Significance: PA = picric acid, 4-NP = p-nitrophenol, m-OH NB = m-hydroxy nitrobenzene).

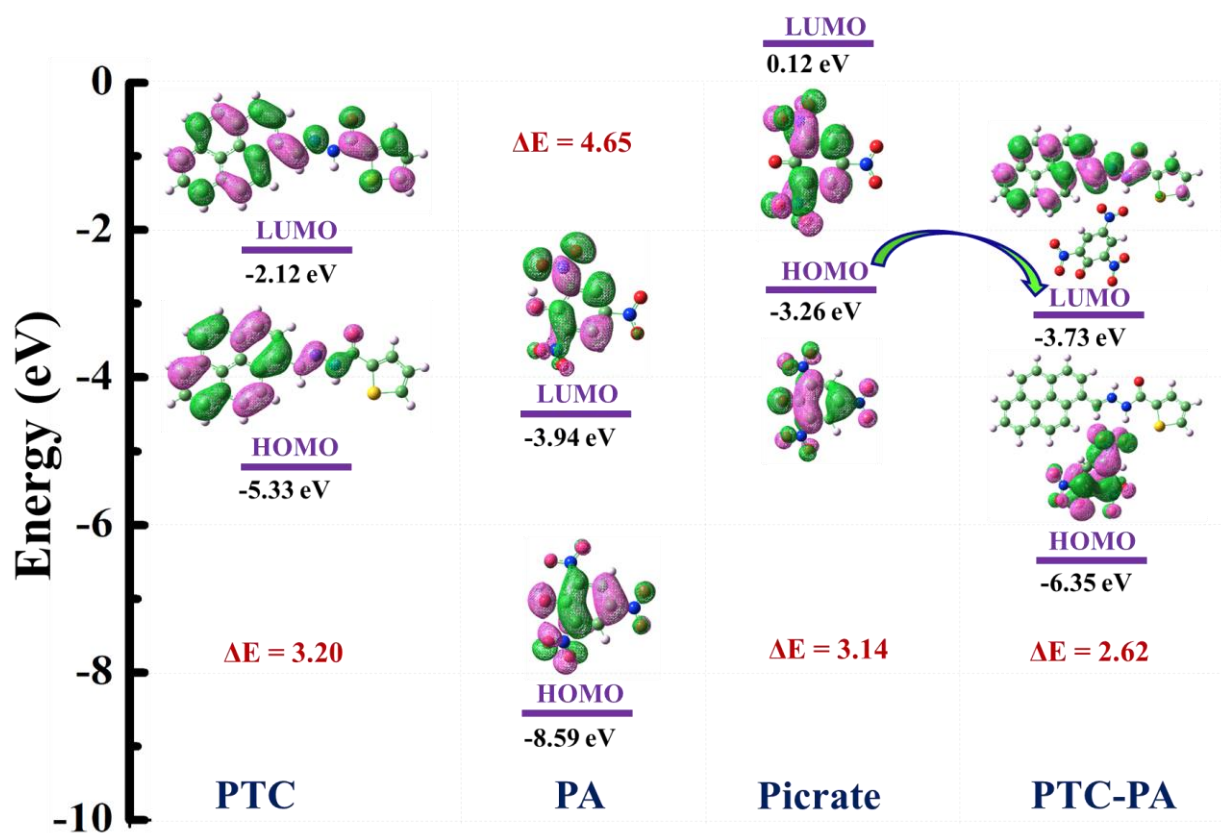


**Fig. S20** Geometry optimized structures, HOMO-LUMO energy levels, band gaps, and the molecular orbital plots of PTC, PA, Picrate, and PTC-PA. All the energies are given in electron volt unit.

**Table S1.** Crystal structure and data refinement for probe PTC

<b>Chemical formula</b>	<b>C<sub>22</sub>H<sub>14</sub>N<sub>2</sub>OS</b>	
<b>Formula weight</b>	354.41 g/mol	
<b>Temperature</b>	293(2) K	
<b>Wavelength</b>	0.71073 Å	
<b>Crystal size</b>	0.330 x 0.260 x 0.210 mm	
<b>Crystal habit</b>	yellowish block	
<b>Crystal system</b>	Monoclinic	
<b>Space group</b>	P 21/c	
<b>Unit cell dimensions</b>	a = 13.6604(4) Å	$\alpha = 90^\circ$
	b = 10.0147(3) Å	$\beta = 99.643(3)^\circ$
	c = 12.6251(3) Å	$\gamma = 90^\circ$
<b>Volume</b>	1702.77(8) Å <sup>3</sup>	
<b>Z, Density (calculated)</b>	4, 1.382 Mg/m <sup>3</sup>	
<b>Absorption coefficient</b>	0.203 mm <sup>-1</sup>	
<b>F(000)</b>	736	
<b>Theta range for data collection</b>	2.876 to 29.009°	
<b>Index ranges</b>	-18 ≤ h ≤ 18, -13 ≤ k ≤ 8, -16 ≤ l ≤ 16	
<b>Absorption correction</b>	Semi-empirical from equivalents	
<b>Max. and min. transmission</b>	0.8390 and 0.7420	
<b>Refinement method</b>	Full-matrix least-squares on F <sup>2</sup>	
<b>Final R indices</b>	R1 = 0.0849, wR2 = 0.2467	
<b>Goodness-of-fit on F<sup>2</sup></b>	1.083	
<b>Data/ restraints/ parameters</b>	4083 / 0 / 235	
<b>CCDC no.</b>	<b>1861748</b>	

**Table S2.** Selective bond lengths and bond angles for PTC

Bond	Length (in Å)	Angles	in deg
<i>S(1)-C(1)</i>	1.681(5)	<i>C(1)-S(1)-C(4)</i>	91.9(2)
<i>S(1)-C(4)</i>	1.711(3)	<i>C(5)-N(1)-N(2)</i>	121.5(3)
<i>O(1)-C(5)</i>	1.243(4)	<i>C(5)-N(1)-H(1N)</i>	119.3
<i>N(1)-C(5)</i>	1.355(4)	<i>N(2)-N(1)-H(1N)</i>	119.3
<i>N(1)-N(2)</i>	1.369(3)	<i>C(6)-N(2)-N(1)</i>	115.6(3)
<i>N(1)-H(1N)</i>	0.8600	<i>C(2)-C(1)-S(1)</i>	113.4(4)
<i>N(2)-C(6)</i>	1.283(4)	<i>S(1)-C(1)-H(1)</i>	123.3

**Table S3.** Summary of solvent dependent absorption maximum and molar extinction coefficient (0.08  $\mu$ M concentration of each solution)

Entry	Solvent	$\lambda_{\text{max}}$ (nm)	$\lambda_{\text{ex}}$ (nm) / OD Value	$\log \epsilon$
<b>01</b>	Acetone	237, 311, 369, 400	<b>369</b> / 0.87585	9.0394
<b>02</b>	Acetonitrile	274, 368, 400	<b>368</b> / 0.81494	9.0081
<b>03</b>	Chloroform	225, 269, 377, 405	<b>377</b> / 0.86612	9.0345
<b>04</b>	Dichloromethane	221, 266, 374, 402	<b>374</b> / 0.96177	9.0799
<b>05</b>	Dimethylformamide	280, 375, 403	<b>375</b> / 0.90657	9.0544
<b>06</b>	Dimethylsulfoxide	280, 381, 405	<b>381</b> / 0.90276	9.0525
<b>07</b>	Ethyl Acetate	234, 273, 368, 400	<b>368</b> / 1.10049	9.1385
<b>08</b>	Ethanol	272, 374, 403	<b>374</b> / 0.97211	9.0847
<b>09</b>	Methanol	267, 371, 403	<b>371</b> / 0.99147	9.0932
<b>10</b>	PBS Buffer	262, 386, 421	<b>386</b> / 0.34839	8.6389
<b>11</b>	Water	260, 371, 403	<b>371</b> / 0.40625	8.7058

**Table S4.** Lifetime decay parameters of sensor PTC upon addition of PA and  $\text{Cu}^{2+}$  ion

System	$\tau_1$ (ns)	$\alpha_1$	$\tau_2$ (ns)	$\alpha_2$	$\tau_3$ (ns)	$\alpha_3$	$\langle \tau \rangle$ (ns)	$\chi^2$
PTC	0.19	0.28	0.38	0.71	0.77	0.01	<b>0.093</b>	1.15
PTC + $\text{Cu}^{2+}$	0.29	0.24	0.58	0.02	1.17	0.74	<b>0.140</b>	1.13
PTC-PA	0.007	0.73	0.15	0.27	0.30	-	<b>0.074</b>	1.06

**Table S5.** The calculated Stern-Volmer quenching constant ( $K_{SV}$  in acetone,  $M^{-1}$ ), and thermodynamics parameters, such as, standard enthalpy change ( $\Delta H$  in  $kJ mol^{-1}$ ), standard entropy change ( $\Delta S$  in  $kJ mol^{-1} K^{-1}$ ), and standard Gibbs free energy change ( $\Delta G$  in  $kJ mol^{-1}$ ) of the PTC-PA adduct.

T (K)	$K_{SV} (\times 10^7) (M^{-1})$	$\Delta H (kJ mol^{-1})$	$\Delta S (kJ mol^{-1} K^{-1})$	$\Delta G (kJ mol^{-1})$
288	$1.13 \pm 0.02$	-81.77	133.89	-120.33
298	$1.92 \pm 0.10$			-121.66
308	$2.22 \pm 0.10$			-123.0

**Table S6.** DFT outcomes and optical properties of PTC, PTC+Cu<sup>2+</sup>, and PTC-PA.

Compound	$E^a$ (Hartrees)	HOMO <sup>b</sup> (eV)	LUMO <sup>b</sup> (eV)	$\Delta E^b$ (eV)	$\Delta E^c$ (eV)	$\lambda_{max}^d$ (nm)		$\lambda_{em}^e$ (nm)	$\Phi_f^f$
						Thr.	Exp.		
PTC	-1429.398	-5.35	-2.12	3.20	3.04	346	368	425	0.007
PTC-PA	-2350.039	-6.35	-3.73	2.62	2.77	337	344	462	-

<sup>a</sup> Overall energy (a.u.)

<sup>b</sup> Different MOs and energy gaps are interpreted *via* B3LYP/6-31G of Gauss 09 software

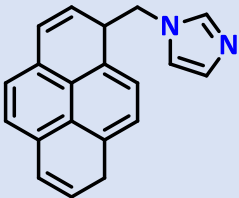
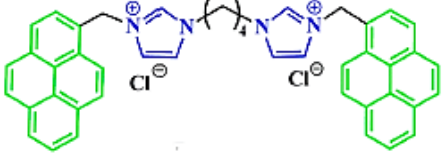
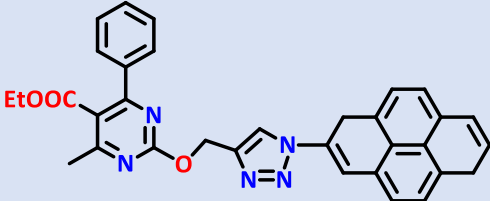
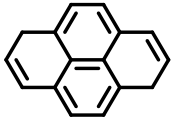
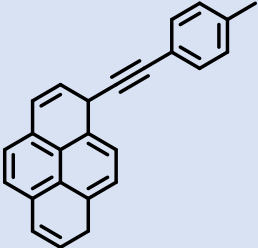
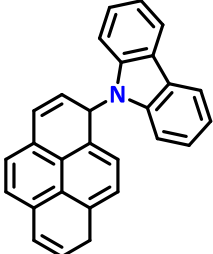
<sup>c</sup> Optical band gap (where,  $\Delta E = LUMO-HOMO$ ) calculated by UV-visible spectra

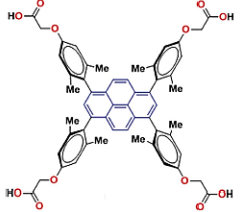
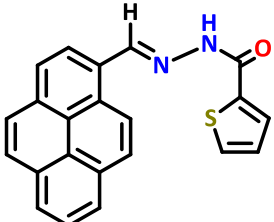
<sup>d</sup> Theoretical (CAMB3LYP/6-31+G) and experimental wavelength maximum (in nm)

<sup>e</sup> Experimental emission wavelength maximum (in nm)

<sup>f</sup> Quantum yield ( $\Phi_f$  of standard Coumarin 152 = 0.09 in MeOH)

**Table S7.** Comparison of LOD and binding constant values of some pyrene based picric acid sensor

Entry	Probe	Solvent	$\lambda_{ex}/\lambda_{em}$ (nm)	LOD	$K_a/K_d/K_{SV}^\dagger$	Ref.
1		Toluene, CH <sub>3</sub> CN	342/ 377, 398	576 ppb	$K_a = 6.58 \times 10^4 \text{ M}^{-1}$	15
2		methanol	345/ 480	$1.0 \times 10^{-6} \text{ M}$	$K_d = 6.58 \times 10^4 \text{ M}$	16
3		THF- HEPES (1/9, v/v, pH=6.99)	342/ 380- 399	1.93 ppb	-	17
4		Ethanol	334/ 393	3.11 ppm	$K_{SV} = 1041 \text{ M}^{-1}$	18
5		Ethanol	362/ 391	3.09 ppm	$K_{SV} = 2720 \text{ M}^{-1}$	
6		Ethanol	344/ 398	2.89 ppm	$K_{SV} = 677 \text{ M}^{-1}$	

7		n-hexane	320/ 410	$5.5 \times 10^{-4} \text{ M}$	$K_{SV} = 178.5 \text{ M}^{-1}$	19
8		CH <sub>3</sub> CN	368/ 425	19 nM	$K_a = 6.814 \times 10^6 \text{ M}^{-1}$	P*
9		THF	375/ 425	1.0 ppm	$K_{SV} = 6.9-8.3 \times 10^3 \text{ M}^{-1}$	20

† Association/ Dissociation/ Stern-Volmer Constant

P\* = Present work

## References

1. S. Guha, S. Lohar, A. Banerjee, A. Sahana, I. Hauli, S. K. Mukherjee, J. S. Matalobos and D. Das, *Talanta*, 2012, 91, 18-25.
2. B. K. Kundu, R. Singh, R. Tiwari, D. Nayak and S. Mukhopadhyay, *New J. Chem.*, 2019, 43, 4867-4877.
3. A. Bhattacharya, R. Prajapati, S. Chatterjee and T. K. Mukherjee, *Langmuir*, 2014, 30, 14894-14904.
4. P. Dahiya, M. Kumbhakar, T. Mukherjee and H. Pal, *Chem. Phys. Lett.*, 2005, 414, 148-154.
5. A. T. R. Williams, S. A. Winfield and J. N. Miller, *Analyst*, 1983, 108, 1067-1071.
6. M. J. Frisch, G. W. Trucks, H. B. Schlegel, G. E. Scuseria, M. A. Robb, J. R. Cheeseman, G. Scalmani, V. Barone, G. A. Petersson, H. Nakatsuji, X. Li, M. Caricato, A. V. Marenich, J. Bloino, B. G. Janesko, R. Gomperts, B. Mennucci, H. P. Hratchian, J. V. Ortiz, A. F. Izmaylov, J. L. Sonnenberg, Williams, F. Ding, F. Lipparini, F. Egidi, J. Goings, B. Peng, A. Petrone, T. Henderson, D. Ranasinghe, V. G. Zakrzewski, J. Gao, N. Rega, G. Zheng, W. Liang, M. Hada, M. Ehara, K. Toyota, R. Fukuda, J. Hasegawa, M. Ishida, T. Nakajima, Y. Honda, O. Kitao, H. Nakai, T. Vreven, K. Throssell, J. A. Montgomery Jr., J. E. Peralta, F. Ogliaro, M. J. Bearpark, J. J. Heyd, E. N. Brothers, K. N. Kudin, V. N. Staroverov, T. A. Keith, R. Kobayashi, J. Normand, K. Raghavachari, A. P. Rendell, J. C. Burant, S. S. Iyengar, J. Tomasi, M. Cossi, J. M. Millam, M. Klene, C. Adamo, R. Cammi, J. W. Ochterski, R. L. Martin, K. Morokuma, O. Farkas, J. B. Foresman and D. J. Fox, Wallingford, CT, 2016.
7. C. Lee, W. Yang and R. G. Parr, *Physical Review B*, 1988, 37, 785-789.
8. H. Guo, Y. Jing, X. Yuan, S. Ji, J. Zhao, X. Li and Y. Kan, *Organic & Biomolecular Chemistry*, 2011, 9, 3844-3853.
9. B. K. Kundu, R. Ranjan, A. Mukherjee, S. M. Mobin and S. Mukhopadhyay, *J. Inorg. Biochem.*, 2019, 195, 164-173.
10. M. Cossi, N. Rega, G. Scalmani and V. Barone, *J. Comput. Chem.*, 2003, 24, 669-681.
11. *SAINT V8.34A; Bruker AXS Inc.*, 2013.
12. *SHELXTL -2014/7; Bruker AXS Inc.*, 2014.
13. B. Kumar Kundu, V. Chhabra, N. Malviya, R. Ganguly, G. S. Mishra and S. Mukhopadhyay, *Micropor. Mesopor. Mat.*, 2018, 271, 100-117.
14. B. K. Kundu, P. Mandal, B. G. Mukhopadhyay, R. Tiwari, D. Nayak, R. Ganguly and S. Mukhopadhyay, *Sensors and Actuators B: Chemical*, 2019, 282, 347-358.
15. R. Sodkhomkhum, M. Masik, S. Watchasit, C. Suksai, J. Boonmak, S. Youngme, N. Wanichacheva and V. Ervithayasuporn, *Sensors and Actuators B: Chemical*, 2017, 245, 665-673.
16. L. Ding, Y. Bai, Y. Cao, G. Ren, G. J. Blanchard and Y. Fang, *Langmuir*, 2014, 30, 7645-7653.
17. R. Chopra, P. Kaur and K. Singh, *Anal. Chim. Acta*, 2015, 864, 55-63.
18. S. Sriyab, K. Jorn-lat, P. Prompinit, P. Wolschann, S. Hannongbua and S. Suramitr, *J. Lumin.*, 2018, 203, 492-499.
19. A. Bajpai, A. Mukhopadhyay, M. S. Krishna, S. Govardhan and J. N. Moorthy, *IUCrJ*, 2015, 2, 552-562.
20. A. F. Khasanov, D. S. Kopchuk, I. S. Kovalev, O. S. Taniya, K. Giri, P. A. Slepukhin, S. Santra, M. Rahman, A. Majee, V. N. Charushin and O. N. Chupakhin, *New J. Chem.*, 2017, 41, 2309-2320.